Nonradiative double-electron capture in fast collisions of bare Xe^{54+} ions with Kr and Xe gaseous targets

Bian Yang,[1,2] Zhongwen Wu,[3] Deyang Yu,[1,2,*] Caojie Shao,[1,2,†] Mingwu Zhang,[1,2] Yingli Xue,[1,2] Wei Wang,[1,2] Zhangyong Song,[1,2] Junliang Liu,[1,2] Fangfang Ruan,[4] Yehong Wu,[5] and Xiaohong Cai[1]

[1]*Institute of Modern Physics, Chinese Academy of Sciences, Lanzhou 730000, China*

[2]*University of Chinese Academy of Sciences, Beijing 100049, China*

[3]*Key Laboratory of Atomic and Molecular Physics & Functional Materials of Gansu Province, College of Physics and Electronic Engineering, Northwest Normal University, Lanzhou 730070, China*

[4]*Department of Medical Imaging, Hangzhou Medical College, Hangzhou 310053, China*

[5]*School of Basic Medical Sciences, Shanxi Medical University, Taiyuan 030001, China*

(Received 15 December 2023; accepted 12 July 2024; published 1 August 2024)

We studied the nonradiative double-electron capture in collisions of 95, 146, and 197 MeV/u Xe^{54+} ions with Kr and Xe atoms by measuring the x-ray intensity ratios $I(1snp \rightarrow 1s^2)/I(np \rightarrow 1s)$ ($n = 2$, 3, and 4) of the resulting Xe^{52+*} and Xe^{53+*} ions. It was found that the double-electron capture becomes more important with decreasing projectile energy, although the single-electron capture is always dominant. At the lower energies of 95 and 146 MeV/u the intensity ratios $I(1s2p \rightarrow 1s^2) : I(1s3p \rightarrow 1s^2) : I(1s4p \rightarrow 1s^2)$ of Xe^{52+*} ions were found to be nearly identical to the ratios $I(2p \rightarrow 1s) : I(3p \rightarrow 1s) : I(4p \rightarrow 1s)$ of Xe^{53+*} ions for the Kr target, which implies that the double-electron capture can be regarded as two uncorrelated one-electron capture processes, whereas this feature disappears for the heavier Xe target. It was also found that at 95 and 146 MeV/u the relative double-electron capture intensity for $Xe^{54+} + Xe$ collisions is significantly larger than that for $Xe^{54+} + Kr$ collisions. We speculate that the resonant electron transfer plays an important role in the symmetric $Xe^{54+} + Xe$ collisions and the double-electron capture therein cannot be regarded as two independent one-electron capture events.

DOI: 10.1103/PhysRevA.110.022801

I. INTRODUCTION

The nonradiative electron capture (NRC) has been known to be the dominant charge-exchange process in fast collisions of highly charged high-Z projectile ions with heavy target atoms [1]. In this process, a bound electron of the target atom is captured into a bound state of the projectile ion without the simultaneous emission of photons and the excess energy and momentum are shared between the target and the projectile [1,2]. It has been also known that the nonradiative double-electron capture (NRDC) process becomes more important as the kinetic energy of projectile ions decreases, the charge state of projectile ions increases, or the nuclear charge of target atoms increases, respectively [3]. Nevertheless, since there are few, if any, appropriate *ab initio* theoretical studies available for the NRDC process, to the best of our knowledge, it is still a challenging task to well understand the fundamental physics involved in the process, such as the relativistic effect, electron-electron interaction, electron correlation effect, distortion of atomic wave functions at large distances caused by the Coulomb field of the energetic high-Z projectile ions, and so on [1,4].

Due to limitations of experimental facilities and techniques, experimental studies of the NRDC process involved in high-energy collisions of bare or H-like high-Z ions with heavy atoms were rarely performed during the past decades. Recently, however, combined with the cooling storage ring of heavy ions [2,5,6] and the gaseous internal target [2,7], NRC and NRDC experiments of high-Z ions under the single-collision condition can be carried out at projectile energies ranging from tens to hundreds of MeV/u [1,3]. Therefore, a few experiments measuring total cross sections and state-selective populations of the NRC and NRDC processes in high-energy collisions of bare, H-like and He-like heavy ions with gaseous atoms have been reported [8–14]. In these collision studies, special attention has been devoted to the production of excited ionic states and to the measurement of their subsequent radiative decay. High-precision measurements of characteristic x-ray emissions from the doubly down-charged projectile ions can not only give access to the investigation of atomic fine-structure levels and electron correlation effects in heavy few-electron systems, but also provide a test of the theoretical models for describing the NRDC dynamics [1,2]. Moreover, the relevant experimental results are also important for the determination of the charge state distribution and the lifetime of stored ion beams in heavy-ion accelerators and cooling storage rings [2,8,15].

Regarding the aspect of theoretical studies on the NRC and NRDC processes, the relativistic eikonal approximation (REA) and the relativistic two-center coupled-channel method can be used to evaluate the NRC cross sections in fast collisions of highly charged ions with atoms [4,16–18], but

*Contact author: d.yu@impcas.ac.cn

†Contact author: c.shao@impcas.ac.cn

they do not work for the calculations of the NRDC cross sections due to the lack of impact-parameter dependence of the capture probabilities into excited states [3,4,19]. In practice, the many-body classical-trajectory Monte Carlo (n-CTMC) method [20] can be used to predict total cross sections for both the NRC and NRDC processes. For example, it has been used to simulate the measured total NRC and NRDC cross sections in collisions of 4–12 MeV/u Ge^{31+} ions with Ne target atoms [14]. It was found that the measured NRC cross sections were reasonably reproduced by the n-CTMC calculations, while the NRDC cross sections obtained with the n-CTMC method were systematically overestimated by a factor of about 1.2–1.6 when compared to the measured ones [14]. In addition, the NRDC process occurring in collisions of fast-moving highly charged heavy ions with heavy atoms may be understandable by means of the independent-electron approximation (IEA) [3,21,22]. For instance, Anholt *et al.* measured NRDC cross sections for 105 MeV/u $U^{83+,\,89+,\,90+,\,91+}$, 220 MeV/u U^{91+}, 82 MeV/u $Xe^{52+,\,53+,\,54+}$, and 140 and 200 MeV/u Xe^{54+} ions passing through Al, Cu, Ag, and Au target foils, respectively [3,22]. These experimental results generally agree with the IEA calculations, which have been adjusted by multiplying appropriate empirical fitting factors due to impact-parameter dependencies of the electron-capture probabilities that were estimated with the Oppenheimer-Brinkman-Kramers (OBK) approximation [1]. Nevertheless, it should be noticed that since solid targets were used in experiments, additional uncertainties caused by the multicollision effect still exist in these experimental results [23].

In this paper, we report on x-ray measurements associated with the nonradiative single- and double-electron capture in collisions of bare Xe^{54+} ions with krypton and xenon atoms at projectile energies of 95, 146, and 197 MeV/u. The experimental relative cross-section ratios for the single- and double-electron capture are compared with theoretical results calculated with the REA and IEA models, respectively. The measured spectral intensity ratios between the $1snp \rightarrow 1s^2$ lines of Xe^{52+*} and the $np \rightarrow 1s$ ($n = 2$, 3, and 4) lines of Xe^{53+*} indicate that the double-electron capture becomes increasingly important with decreasing projectile energy from 197 to 95 MeV/u, although the single-electron capture remains always to be the dominant charge-exchange process within the energy range considered. Furthermore, the experimental NRDC results obtained for different target atoms and projectile energies reveal target-atomic-number and energy dependencies of populating excited projectile states, respectively. Moreover, for the Kr target, the experimental results show that a double-electron capture event can be regarded as two uncorrelated single-electron capture processes. However, the results obtained for the Xe target (i.e., for a symmetric collision of heavy elements) could provide certain information on the possibility that the double-electron capture process in the symmetric $Xe^{54+} + Xe$ collisions cannot be regarded as two independent one-electron capture events and the resonant electron transfer probably plays an important role therein.

The paper is organized as follows. The experiment and data analysis are described in the next section. The results and discussion are presented in Sec. III. Finally, a brief conclusion is given in Sec. IV.

II. EXPERIMENT AND DATA ANALYSIS

The experiment was performed at the Heavy Ion Research Facility at Lanzhou-Cooling Storage Ring (HIRFL-CSR) [5,6]. Since a detailed description of the experimental setup used in this study can be found in Refs. [10,11,24], here we just briefly summarize the major aspects. Around 10^7 bare xenon ions were stored and cooled in the experimental ring of the HIRFL-CSR. To induce and measure the electron capture process, the internal supersonic jet target was used and overlapped with the stored ion beam in a perpendicular direction. The experiment was performed for Kr and Xe targets at three beam energies of 95, 146, and 197 MeV/u. The target area densities were between 10^{12} and 10^{13} atoms/cm^2, and therefore the single-collision condition was well satisfied according to the total electron-capture cross section of around 10^{-19}–10^{-20} cm^2 in the present experiment [3,4,16,17]. In order to measure projectile x rays radiated in the electron capture process and the subsequent decay of the excited states of the down-charged projectile ions, the beam-target interaction zone was observed by four high-purity germanium (HPGe) detectors and two lithium-drifted silicon [Si(Li)] detectors, which cover observation angles in the range between 35 ° and 145 ° with respect to the ion beam direction. The typical energy resolution (i.e., the full width at half maximum) of the present detectors was about 300 eV at around 30 keV [11]. The solid angles ($\Delta\Omega/4\pi$) covered by the individual detectors were on the order of 10^{-6}–10^{-4}.

As an example, Fig. 1 displays the measured x-ray spectra radiated in the subsequent radiative decay of singly and doubly down-charged Xe^{53+*} and Xe^{52+*} ions following single- and double-electron capture into projectile ions, which were recorded at an observation angle of 60 ° in collisions of bare xenon ions with a krypton target for projectile beam energies of 95, 146, and 197 MeV/u. As shown by Fig. 1, the single-electron capture is found to be clearly dominant in the collisions at all of the projectile energies considered. In particular, the contribution of the double-electron capture is almost invisible at the projectile energy of 197 MeV/u. The measured spectra show the radiative transitions of Xe^{53+*} and Xe^{52+*} ions from the captured np and $1snp$ configurations to their ground states (referred to as ground-state transitions hereafter).

In the measured x-ray spectra, the Lyman transitions of singly down-charged Xe^{53+*} ions are identified to be caused nearly by the NRC mechanism. Such an identification is based on the fact that no photon emission associated with the radiative electron capture (REC) of Xe^{54+} ions is observed in experiments, which is also supported by a comparison of the corresponding theoretical NRC and REC cross sections as described in Refs. [10,11]. In addition, the measured K-shell radiations of doubly down-charged Xe^{52+*} ions resulting from the NRDC process are found to prevail dominantly over all other possible mechanisms. The reasons are as follows. First, in the present experiment, especially for heavy targets, the cross sections of the double radiative electron capture (DREC) in collisions of 90–200 MeV/u Xe^{54+} with Kr or Xe are four to seven orders of magnitude smaller than the NRC cross sections calculated with the REA method [4,16,17], where a numerical evaluation of the DREC cross sections [4,25] can

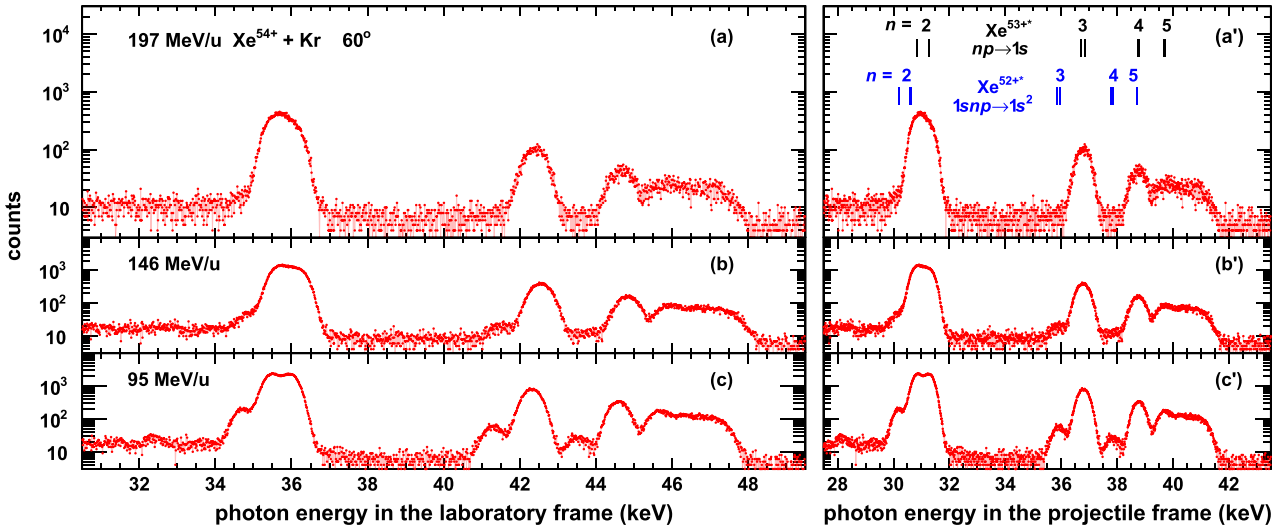

FIG. 1. X-ray spectra measured at an observation angle of 60 ° in collisions of Xe^{54+} ions with Kr atoms. The x-ray photons are emitted in the subsequent radiative decay of down-charged projectile ions following single- and double-electron capture into excited projectile ions. The spectra are presented, respectively, in the laboratory (left panel) and projectile (right) frames for three projectile energies of 197 MeV/u [(a),(a′)], 146 MeV/u [(b),(b′)], and 95 MeV/u [(c),(c′)]. The radiative transitions $1snp \rightarrow 1s^2$ ($n = 2$, 3, 4, and 5) of doubly down-charged Xe^{52+*} ions and $np \rightarrow 1s$ of singly down-charged Xe^{53+*} ions are indicated by vertical lines in the right panel.

be obtained with the use of the corresponding REC cross sections based on a nonrelativistic dipole approximation as introduced in Ref. [2]. Thus, the DREC process is negligible in the present work because the observed transition lines originating from double-electron capture are approximately one to two orders of magnitude smaller than those originating from single-electron capture at 95 and 146 MeV/u (as shown in Fig. 1). Second, the cross sections of the radiative double-electron capture (RDEC) are two to three orders of magnitude smaller than those of the DREC mechanism [25–27]. Third, the double capture mechanism with emission of one photon (i.e., one of the target electrons is captured by the NRC process and simultaneously the other is captured by the REC mechanism in a single collision) can be ignored since no corresponding photon emission can be identified in the measured x-ray spectra. For the above reasons, in the following analysis the x-ray emissions of the doubly down-charged Xe^{52+*} ions are considered to result only from the NRDC mechanism.

As seen from Fig. 1, the photon energies of the Lyman transitions $np \rightarrow 1s$ ($n = 2$, 3, and 4) of Xe^{53+*} ions are just slightly larger than those of the $1snp \rightarrow 1s^2$ ($n = 2$, 3, and 4) transitions of Xe^{52+*} ions. Here it should be noted that other (higher-) multipole radiative transitions from the ns ($n \geqslant 2$) and nd ($n \geqslant 3$) levels of Xe^{53+*} ions as well as the $1sns$ ($n \geqslant 2$) and $1snd$ ($n \geqslant 3$) levels of Xe^{52+*} ions may also contribute to the observed overall spectra of the down-charged projectile ions produced by the NRC and NRDC mechanisms. Nevertheless, the mixture of them in the present work cannot be resolved because of additional broadening introduced by the Doppler effect of fast projectiles and limited energy resolution of the photon detectors used in experiments. Therefore, in the present experiment the observed transitions $1snp \rightarrow 1s^2$ ($n = 2$, 3, and 4) of Xe^{52+*} ions represent all the ground-state decays from KL, KM, and KN shells of Xe^{52+*} ions, while the transitions $np \rightarrow 1s$ ($n = 2$, 3, and 4) of Xe^{53+*} ions are involved in all the decays from L, M, and N shells of Xe^{53+*} ions. We note that these transitions in 50 MeV/u Xe^{54+} + Xe collisions have been resolved by using a cryogenic calorimeter detector [30]. In addition, based on the REA cross sections calculated for the NRC to the K, L, M, and N shells of the projectile in collisions of 90–200 MeV/u Xe^{54+} ions with Kr and Xe targets (as reported in our previous studies [10,11]), single-electron capture into the ground state of singly down-charged Xe^{53+} ions is found to be dominant (the contribution by capture into the L shell is obviously small and the cross sections of electron capture to the M and N shells are much smaller than that to the L shell), whereas the double-electron capture into the doubly excited states $nln'l'$ (n, $n' > 1$) of Xe^{52+*} ions is estimated with the IEA to be unimportant and thus can be ignored in the present work. For revealing state-selective information about the NRC and NRDC processes, the number of counts (i.e., intensity) recorded for the $np \rightarrow 1s$ and $1snp \rightarrow 1s^2$ ($n = 2$, 3, and 4) lines is obtained by fitting the corresponding peaks in the spectra with Gaussian functions and a linear background, as described in detail in Ref. [11]. Figure 2 shows an example of determining intensities of the spectral lines $1s2p \rightarrow 1s^2$ of Xe^{52+*} ions and $2p \rightarrow 1s$ of Xe^{53+*} ions measured in collisions of 95, 146, and 197 MeV/u Xe^{54+} with Xe at an observation angle of 35 °. Obviously, the subsequent radiative decay associated with the NRC into the projectile ions dominates the measured x-ray spectra. In contrast, at the projectile energy of 197 MeV/u the contribution of the NRDC is found to be negligible. As the projectile energy decreases to 146 MeV/u, the fitting peaks resulting from the NRDC become clearly visible. At the lowest energy of 95 MeV/u considered, the peak intensities originating from the NRDC are further enhanced.

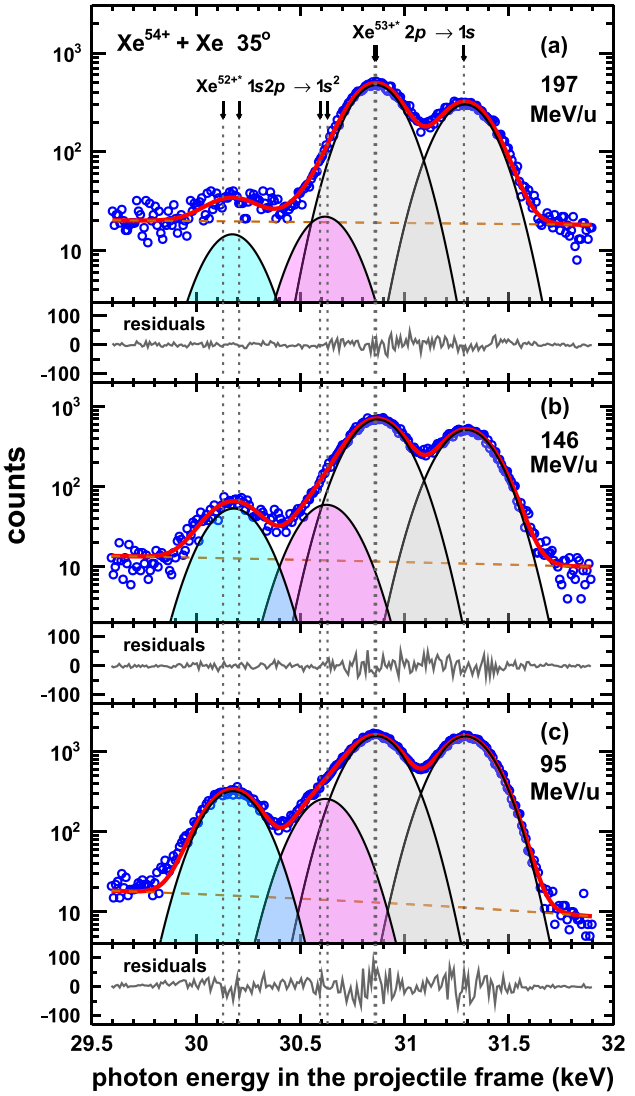

FIG. 2. X-ray spectra from the ground-state transitions $1s2p \rightarrow 1s^2$ of Xe^{52+*} ions as well as $2p \rightarrow 1s$ of Xe^{53+*} ions produced in collisions of projectile Xe^{54+} ions with the Xe target, which are recorded at an observation angle of 35 ° for three projectile energies: (a) 197, (b) 146, and (c) 95 MeV/u. The transitions resulting from both the NRDC and NRC are labeled the same as in Fig. 1, and the corresponding transition energies of excited Xe^{52+} [28] and Xe^{53+} [29] ions are also illustrated by dashed vertical lines. With the use of the corresponding transition energies and detector energy resolution, the intensities of these peaks are determined by a fitting procedure with four Gaussian functions [i.e., $2p_{3/2} \rightarrow 1s_{1/2}$, $2p_{1/2} \rightarrow 1s_{1/2}$ mixed with $2s_{1/2} \rightarrow 1s_{1/2}$, $(1s_{1/2}2p_{3/2})_1 \rightarrow 1s^2$ mixed with $(1s_{1/2}2p_{3/2})_2 \rightarrow 1s^2$, and $(1s_{1/2}2p_{1/2})_1 \rightarrow 1s^2$ mixed with $(1s_{1/2}2s_{1/2})_1 \rightarrow 1s^2$] and a linear background. The intensity, width, and position of the Gaussian peaks are adjustable parameters. Since the width of the peaks is defined by the detector resolution and the Doppler broadening in this energy region, it is set to be a common free parameter. The spacing ratio for the positions of these peaks is fixed according to the corresponding transition energies for minimizing fitting uncertainty, as described in Refs. [10–12]. The respective fitting residuals are shown in the lower part of each panel. The obtained intensities of these peaks are then corrected for the energy-dependent detection efficiency (with an error of 3% for this correction).

III. RESULTS AND DISCUSSION

The experimental excited-state population for double-electron capture can be determined by means of the intensity ratios $I(1snp \rightarrow 1s^2)/I(np \rightarrow 1s)$ ($n = 2$, 3, and 4) of Xe^{52+*} and Xe^{53+*} ions produced in collisions of 95, 146, and 197 MeV/u bare xenon ions with krypton or xenon atoms. This scheme of normalizing the intensities of energetically close transition lines allows us to reduce the influence of possible systematic uncertainties (such as those caused by the solid angles of detectors and the difference of detection efficiencies) [2,31]. As an example, Fig. 3 illustrates the intensity ratios $I(1s2p \rightarrow 1s^2)/I(2p \rightarrow 1s)$, $I(1s3p \rightarrow 1s^2)/I(3p \rightarrow 1s)$, and $I(1s4p \rightarrow 1s^2)/I(4p \rightarrow 1s)$ measured in collisions of 95 MeV/u Xe^{54+} ions with Kr and Xe targets, as functions of the laboratory observation angle θ_{lab}. Since no significant anisotropy is observed for the intensity ratios of these x-ray lines, in the present work these intensity ratios are treated as constants with respect to the observation angle. To be specific, such constants (i.e., the overall intensity ratios) are obtained by weighted averaging of the measured x-ray intensity ratios at all the observation angles with their respective statistics. The uncertainties of the overall intensity ratios were obtained by propagation from errors of corresponding x-ray intensity ratios at each observation angle, which were estimated from the statistics of data and the fitting procedure. The statistics of data was deduced from the square root of intensity of the transition peak, and the fitting uncertainties were evaluated by means of the fitting residuals. As seen from the figure, the intensity ratio $I(1s2p \rightarrow 1s^2)/I(2p \rightarrow 1s)$ for the Xe target is significantly larger than those for other cases. For example, the intensity ratios $I(1s3p \rightarrow 1s^2)/I(3p \rightarrow 1s)$ and $I(1s4p \rightarrow 1s^2)/I(4p \rightarrow 1s)$ for the same Xe target are almost the same as each other and both are smaller than the ratio $I(1s2p \rightarrow 1s^2)/I(2p \rightarrow 1s)$ by $\sim 40\%$. As for the Kr target, the three intensity ratios $I(1snp \rightarrow 1s^2)/I(np \rightarrow 1s)$ ($n = 2$, 3, and 4) are nearly identical to each other and are smaller by $\sim 60\%$. In addition, it is worth mentioning that the projectile Lyman-α_1 line following the NRC of bare Xe^{54+} ions exhibits a visible anisotropic angular distribution at low projectile energies and the $2p \rightarrow 1s$, $3p \rightarrow 1s$, and $4p \rightarrow 1s$ transition lines following the same NRC mechanism roughly have the same angular emission pattern, as shown in our previous studies [10,12]. Therefore, the $1s2p \rightarrow 1s^2$, $1s3p \rightarrow 1s^2$, and $1s4p \rightarrow 1s^2$ transition lines following the NRDC of Xe^{54+} ions are estimated to have angular emission patterns similar to that of the $2p \rightarrow 1s$ line, considering that their intensity ratios are found to be isotropic.

Figure 4 displays the measured intensity ratios $I(1snp \rightarrow 1s^2)/I(np \rightarrow 1s)$ ($n = 2$, 3, and 4) of the x-ray lines of Xe^{52+*} and Xe^{53+*} ions produced by the NRDC and NRC mechanisms in collisions of bare Xe^{54+} ions with the Kr target, as functions of the projectile velocity. Moreover, when compared to the measured results for the xenon target, a target-atomic-number dependence is also shown. Note that here the measured intensity ratios are plotted as functions of the projectile velocity rather than the projectile energy as used above, which enables direct comparison with the orbital velocity of the target K-shell electron. It is found

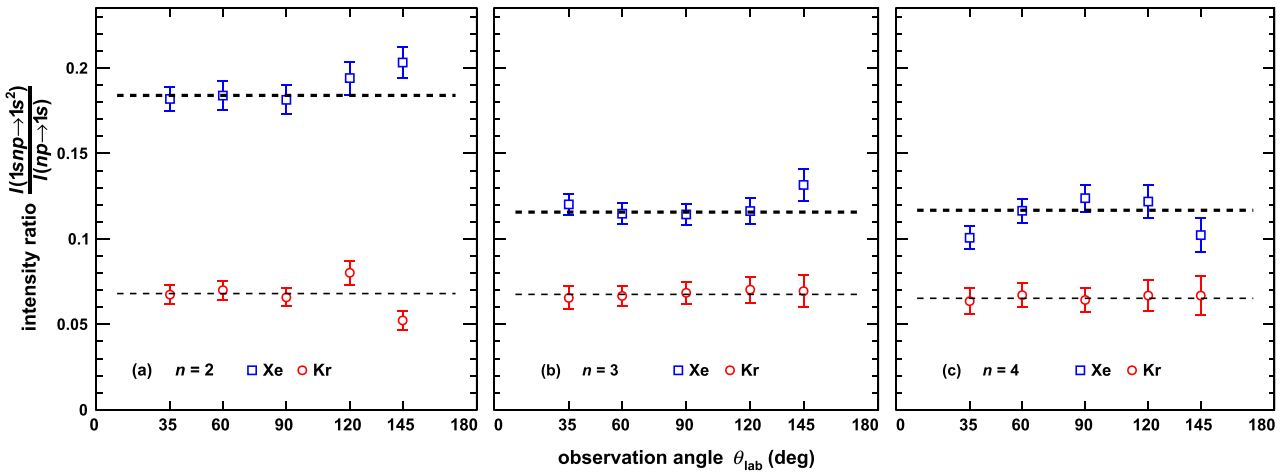

FIG. 3. Experimental x-ray intensity ratios $I(1s2p \to 1s^2)/I(2p \to 1s)$ (a), $I(1s3p \to 1s^2)/I(3p \to 1s)$ (b), and $I(1s4p \to 1s^2)/I(4p \to 1s)$ (c) of Xe^{52+*} and Xe^{53+*} ions as functions of the laboratory observation angle θ_{lab}. Results are shown for collisions of 95 MeV/u Xe^{54+} ions with Kr (red circles) and Xe (blue squares) targets. The error bars are estimated from the statistics of data and the fitting procedure. The dashed lines indicate weighted average values of the intensity ratios (i.e., the overall intensity ratios).

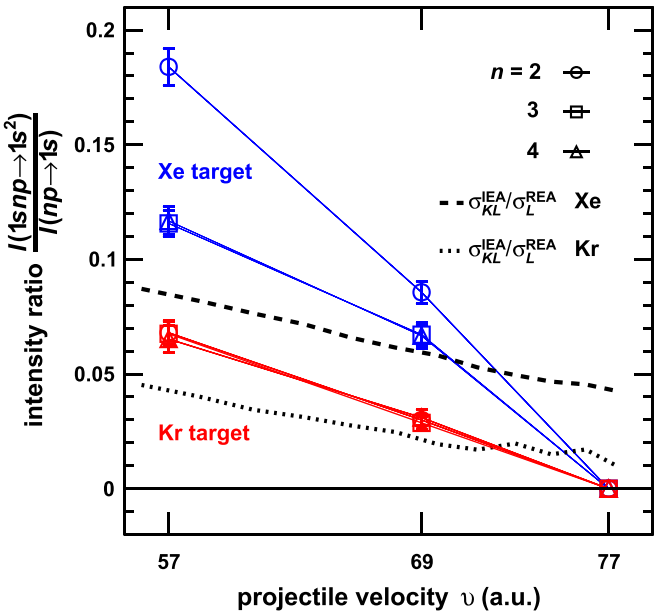

FIG. 4. Experimental x-ray intensity ratios $I(1snp \to 1s^2)/I(np \to 1s)$ ($n = 2$, 3, and 4) of Xe^{52+*} and Xe^{53+*} ions produced by the NRDC and NRC mechanisms in collisions of bare Xe^{54+} ions with Kr (red symbols) and Xe (blue symbols) targets at the projectile velocities of 57, 69, and 77 a.u., which correspond to the projectile energies of 95, 146, and 197 MeV/u, respectively. The thin solid lines connecting the experimental data are meant to guide the eyes. The experimental error bars are estimated from the statistics of data and the fitting procedure. To compare with the measured intensity ratios, theoretical relative cross sections $\sigma_{KL}^{IEA}/\sigma_{L}^{REA}$ of the NRDC into the KL shells and the NRC into the L shell are plotted as an example for Xe (dashed line) and Kr (dotted line) targets, which are calculated, respectively, using the IEA and the REA without taking into account the cascade feeding effect.

that with increasing projectile velocity the line intensities corresponding to the NRDC decrease much more significantly than those corresponding to the NRC for both targets when compared with the velocity dependence of the excited-state populations of the singly down-charged projectile Xe^{53+*} ions (see Fig. 6 of Ref. [11]). In particular, at the highest projectile velocity of 77 a.u. considered at present almost no NRDC events are recorded. Furthermore, for both the Kr and Xe targets the measured intensity ratios are found to be almost linearly dependent upon the projectile velocity, especially for the lighter Kr target. Moreover, the measured x-ray intensity ratios for the Xe target decrease obviously faster than those for the Kr target, in particular, which is the most pronounced for the ratio $I(1s2p \to 1s^2)/I(2p \to 1s)$. To be more specific, at the projectile velocities of 57 and 69 a.u. the intensity ratios for the heavier Xe target are about 2–3 times larger than those for the lighter Kr target.

Below, we shall make a deeper analysis on the measured x-ray line intensities. As seen clearly from Fig. 4, for the Kr target the three intensity ratios $I(1snp \to 1s^2)/I(np \to 1s)$ ($n = 2$, 3, and 4) are determined to be consistent with each other at both of the considered projectile velocities of 57 and 69 a.u. That is to say, the x-ray intensity ratio $I(1s4p \to 1s^2) : I(1s3p \to 1s^2) : I(1s2p \to 1s^2)$ is fully equal to $I(4p \to 1s) : I(3p \to 1s) : I(2p \to 1s)$. This feature implies that the (relative) population of one-electron capture into the L-, M-, or N-shell excited states of the projectile ion is not affected by whether or not another target electron is simultaneously captured into the K shell of the same projectile ion. From this point of view, these double-electron capture processes may be regarded as two (uncorrelated) independent one-electron capture processes in the present work. In contrast, such a feature does not hold for the heavier Xe target as the intensity ratio $I(1s2p \to 1s^2)/I(2p \to 1s)$ is significantly larger than the other two ratios $I(1s3p \to 1s^2)/I(3p \to 1s) \approx I(1s4p \to 1s^2)/I(4p \to 1s)$ at both the projectile velocities.

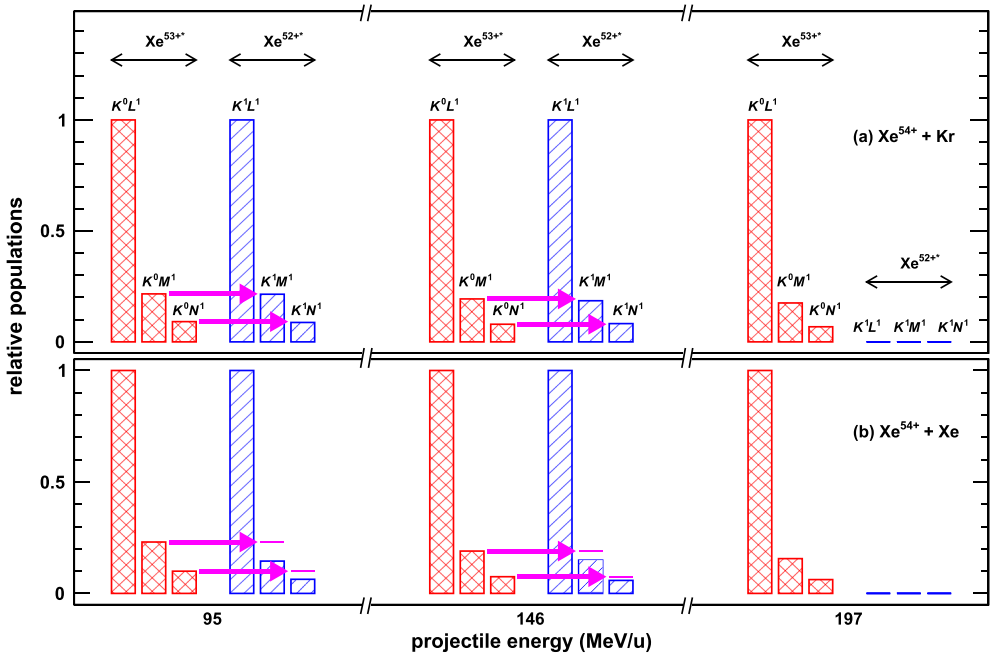

FIG. 5. Relative populations of the excited states of projectile Xe^{52+*} and Xe^{53+*} ions produced in collisions of 95 (left panel), 146 (middle), and 197 MeV/u (right) Xe^{54+} ions with (a) Kr and (b) Xe targets, which are determined by means of the measured x-ray intensities. Note that the populations of the K^1L^1, K^1M^1, and K^1N^1 states of Xe^{52+*} ions resulting from the NRDC are normalized with respect to that of the K^1L^1 state, while the populations of the K^0L^1, K^0M^1, and K^0N^1 states of Xe^{53+*} ions resulting from the NRC are normalized with respect to that of the K^0L^1 state. Here, K^1L^1 denotes that one target electron is captured into the K shell together with another into the L shell, and other notations have similar meanings. The magenta arrows label the relative (normalized) populations of the K^0M^1 and K^0N^1 states of Xe^{53+*} ions at the projectile energies of 95 and 146 MeV/u for both targets, respectively.

In order to analyze the present experimental results, we calculate the NRC cross sections with the use of the REA [4,16,17], and also estimate the NRDC cross sections with the IEA [3,22]. As an example, the calculated relative cross sections $\sigma_{KL}^{\rm IEA}/\sigma_{L}^{\rm REA}$ for the NRDC into the KL shells and the NRC into the L shell are shown in Fig. 4, which are compared with the measured intensity ratios $I(1s2p \rightarrow 1s^2)/I(2p \rightarrow 1s)$ for both the Xe and Kr targets. It should be noted that the theoretical cross sections are calculated without considering the cascade feeding effect, whereas the experimental results incorporate the contribution of such an effect. It is found that the theoretical prediction fails to reproduce the experimental results, although it indeed exhibits a similar linear dependence tendency on the projectile velocity. To be more specific, when compared with the measured intensity ratios the calculated results of $\sigma_{KL}^{\rm IEA}/\sigma_{L}^{\rm REA}$ are underestimated at the projectile velocities of 57 or 69 a.u., but overestimated at the velocity of 77 a.u. for both targets. Moreover, it is also found that the discrepancy between the measured and calculated results for the lighter Kr target is much smaller than for the heavier Xe target, although the theoretical results exhibit nearly parallel velocity-dependence curves for the two targets (because the initial and final states of the captured electrons are described by one-electron wave functions with constant effective nuclear charges at different collision velocities in the present calculations). Here it is worth pointing out that the presently used REA and IEA approaches are not accurate enough to explain the present measurements in detail. To be specific, for the single-electron capture the "higher-potential" prescription of the REA is adopted. However, since the REA is usually applicable for asymmetric high-energy collisions, it is expected to be roughly valid for electron transfer between different target and projectile shells in collisions of Xe^{54+} with the Xe target. Moreover, for the double-electron capture process the infinite-source–infinite-sink model on the basis of the IEA is often employed [3]. However, the OBK capture probabilities were used to evaluate the NRDC cross sections. Even so, there is still a lack of the capture probabilities into higher excited states of the projectile ions and this is why only the cross sections $\sigma_{KL}^{\rm IEA}$ are given in Fig. 4.

To explicitly illustrate energy and target dependencies of the L-, M-, and N-shell populations of projectile Xe^{52+*} and Xe^{53+*} ions produced by the NRDC and NRC mechanisms, respectively, Fig. 5 displays the (relative) populations of the excited states of projectile Xe^{52+*} and Xe^{53+*} ions produced by single- and double-electron capture in collisions of 95, 146, and 197 MeV/u Xe^{54+} ions with Kr and Xe targets, which are determined by means of the measured x-ray intensities. It should be noted that the populations of the K^1L^1, K^1M^1, and K^1N^1 states (with one K-shell vacancy) of Xe^{52+*} ions are normalized with respect to that of the K^1L^1 state, while the ones of the K^0L^1, K^0M^1, and K^0N^1 states (with two K-shell vacancies) of Xe^{53+*} ions are normalized to that of the K^0L^1 state, where K^1L^1 denotes that one target electron is captured into the K shell together with another into the L shell and other notations have similar meanings. As shown by Fig. 5, in collisions of 95 MeV/u Xe^{54+} with the Kr target the (relative)

population of the K^0M^1 state of Xe^{53+*} ions is nearly the same as that of the K^1M^1 state of Xe^{52+*} ions, which holds true also for the K^0N^1 and K^1N^1 states. This pattern supports the finding that the associated double-capture mechanism is the result of two uncorrelated one-electron capture processes. In contrast, in collisions of the same 95 MeV/u Xe^{54+} with the heavier Xe target the corresponding K^0M^1 and K^0N^1 populations of Xe^{53+*} ions are clearly larger than those of Xe^{52+*} ions, respectively, as indicated by the magenta arrows. Thus a difference in the relative population of the projectile excited states produced especially by the double-capture mechanism is obtained between the Kr and Xe targets. For higher projectile energy of 146 MeV/u all the qualitative features identified above remain similar although the specific values are more or less different. To be specific, at both the projectile energies of 95 and 146 MeV/u, the (relative) K^1M^1 and K^1N^1 populations are nearly 20% and 10% of the K^1L^1 population for the Kr target, respectively, whereas they are obviously smaller for the Xe target. The above analysis of the experimental results clearly shows that in the double-electron capture process another target electron is preferentially populated into an energetically lower state when one is captured into the ground state, which is more pronounced for the heavier Xe target. Moreover, at the highest energy of 197 MeV/u considered the NRDC process is not observed for both targets due to no corresponding x-ray emissions from the K^1L^1, K^1M^1, and K^1N^1 states of Xe^{52+*} ions.

Up until now it has hardly been possible to precisely describe the NRDC process in collisions of fast-moving bare high-Z ions with heavy atoms as considered in the present experiment due to the lack of an applicable theory. Therefore, it is still challenging to quantitatively analyze the reasons behind the differences in the NRDC process obtained between the Xe^{54+} + Kr and Xe^{54+} + Xe collisions. Nevertheless, we speculate that the resonant electron transfer may play an important role in the differences among the ratios $I(1snp \rightarrow 1s^2)/I(np \rightarrow 1s)$ ($n = 2$, 3, and 4) at a certain projectile energy in symmetric Xe^{54+} + Xe collisions, while the ratios are almost identical in Xe^{54+} + Kr collisions (as shown in Fig. 4). In the present work, NRDC was observed at the projectile velocities of 57 and 69 a.u., which are much larger than the orbital velocities of the electrons in the target Kr atoms. Besides, the energy levels of the projectile ion Xe^{54+} do not match with those of the target Kr atom (i.e., the binding energy of the exchanged electron initially bound to the target atom is not equal to that of the electron finally captured into the projectile ion). In addition, the projectile nuclear charge is larger than that of the target nucleus, and hence the interaction between the projectile and the target electron is stronger than the one between the target nucleus and the electron during the collision. Therefore, the target electrons can be regarded to be independent during the collision and hence the transfer of electrons in Xe^{54+} + Kr collisions can be expected to be uncorrelated. This may explain the identity of the ratios $I(1snp \rightarrow 1s^2)/I(np \rightarrow 1s)$ ($n = 2$, 3, and 4) at each projectile velocity. However, for the symmetric Xe^{54+} + Xe collisions the situation is different. First, the projectile nuclear charge is the same as the target nuclear charge, and hence the interaction between the projectile and the target electron is as important as the interaction between the target nucleus and the electron. Second, as the corresponding energy levels between the projectile ion and the target atom match (i.e., K-K level matching, and L-L level quasimatching due to the shielding effect of inner-shell electrons on the nucleus), the electron transfer of K-K and L-L is resonant to a large extent. Moreover, the projectile velocities are comparable in magnitude to the orbital velocities of the K-shell target electrons. Therefore, the K-K resonant electron transfer is the most important, and the L-L capture is also important in Xe^{54+} + Xe collisions especially at the energy of 95 MeV/u. For NRC into the M- and N-shell of projectile ions, the resonant capture may be unimportant since the level matching conditions do not exist and the projectile velocities are much higher than the orbital velocities of M- and N-shell electrons for the Xe atom in the present work. In a resonant electron transfer process, the target nucleus plays an important role by means of the energy levels of bound electrons. Since the transfer of an electron changes the corresponding levels, it may affect level matching conditions of the other electrons. Therefore, the population of a captured electron might be different in the cases with or without another electron being captured into the projectile K shell, as observed in the present work. This could explain the enhanced ratios $I(1s2p \rightarrow 1s^2)/I(2p \rightarrow 1s)$ when compared to other ratios in Xe^{54+} + Xe collisions. Furthermore, it is noted that single-electron capture directly into the ground state cannot give rise to subsequent x-ray emission, which appears only if another electron is simultaneously captured into excited states of the projectile ions (i.e., in the double-electron capture), for example, the ground-state decays from KL, KM, and KN shells of Xe^{52+*} ions as observed in the present work. To be specific, only if a simultaneous capture of another electron (into higher shells) occurs, the electron capture into the K shell of the projectile ion would be observed. This could be one explanation for the increased intensity ratios between NRDC and NRC observed in the experiment for the Xe target when compared to the Kr target. Since there are few experimental studies on the double-capture process occurring in relativistic collisions of bare and H-like high-Z ions with gaseous targets to date, we hope that the present experimental NRDC data could serve as a test for relevant theories and also the present work could inspire additional experimental studies of this kind. In addition, more sophisticated and applicable relativistic theories would be highly demanding to quantitatively unravel physical reasons behind the NRDC mechanism in relativistic collisions of heavy ions with targets.

IV. CONCLUSION

To summarize, the nonradiative double-electron capture process has been studied by analyzing the measured x-ray intensity ratios $I(1snp \rightarrow 1s^2)/I(np \rightarrow 1s)$ ($n = 2$, 3, and 4) of the down-charged Xe^{52+*} and Xe^{53+*} ions that are produced in collisions of 95, 146, and 197 MeV/u Xe^{54+} ions with Kr and Xe gaseous atoms. The experimental results indicate that the double-electron capture process becomes more and more pronounced with decreasing projectile energy, although the associated single-electron capture is always dominant for all the collision situations considered above.

To be more specific, the double-electron capture is hardly visible at the projectile energy of 197 MeV/u for both the Kr and Xe targets. In contrast, at the lower projectile energies of 95 and 146 MeV/u the intensity ratios $I(1s2p \rightarrow 1s^2) : I(1s3p \rightarrow 1s^2) : I(1s4p \rightarrow 1s^2)$ are found to be nearly identical to the ratios $I(2p \rightarrow 1s) : I(3p \rightarrow 1s) : I(4p \rightarrow 1s)$ for the Kr target, which indicates that the double-electron capture can be regarded as two uncorrelated one-electron capture processes. However, this feature disappears for the Xe target. Moreover, at 95 and 146 MeV/u the relative intensity of the double-electron capture for symmetric $Xe^{54+} + Xe$ collisions is significantly larger than that for $Xe^{54+} + Kr$ collisions. By means of these experimental findings we speculate that the resonant electron transfer plays an important role therein and the double-electron capture cannot be regarded as two independent one-electron capture events. In addition, the present experimental results could be also used to reveal the excited-state formation mechanism of projectile ions associated with the NRDC in collisions of high-Z ions with heavy atoms at those projectile velocities comparable to the orbital velocities of inner-shell electrons of both the projectile ions and target atoms. Finally, as an obvious difference is found for the Xe target between the present experimental results and the calculated NRDC and NRC cross sections with the use of the IEA and REA approaches, we hope the present work could inspire further interest in performing more NRDC measurements and also developing more applicable relativistic methods to solve the existing difference.

ACKNOWLEDGMENTS

We thank the crew of the accelerator department for their operation of the Heavy Ion Research Facility at Lanzhou-Cooling Storage Ring. This work was supported by the National Key Research and Development Program of China under Grant No. 2022YFA1602500; the "Light of West China" Program of Chinese Academy of Sciences under Grant No. xbzglzb2022004; the National Natural Science Foundation of China under Grants No. 12375263, No. 12375262, No. 12174315, No. 12275328, No. 12175286, No. 11674333, and No. 11905118; and the Outstanding Youth Fund of the Science and Technology Project of Gansu Province under Grant No. 23JRRA687.

[1] J. Eichler and W. E. Meyerhof, *Relativistic Atomic Collisions* (Academic Press, New York, 1995).

[2] J. Eichler and Th. Stöhlker, Radiative electron capture in relativistic ion–atom collisions and the photoelectric effect in hydrogen-like high-Z systems, Phys. Rep. **439**, 1 (2007).

[3] R. Anholt, W. E. Meyerhof, X.-Y. Xu, H. Gould, B. Feinberg, R. J. McDonald, H. E. Wegner, and P. Thieberger, Atomic collisions with relativistic heavy ions. VIII. Charge-state studies of relativistic uranium ions, Phys. Rev. A **36**, 1586 (1987).

[4] W. E. Meyerhof, R. Anholt, J. Eichler, H. Gould, Ch. Munger, J. Alonso, P. Thieberger, and H. E. Wegner, Atomic collisions with relativistic heavy-ions. III. Electron capture, Phys. Rev. A **32**, 3291 (1985).

[5] W. L. Zhan *et al.*, Progress in HIRFL-CSR, Nucl. Phys. A **834**, 694c (2010).

[6] J. W. Xia *et al.*, The heavy ion cooler-storage-ring project (HIRFL-CSR) at Lanzhou, Nucl. Instrum. Methods Phys. Res., Sect. A **488**, 11 (2002).

[7] X. Cai, R. Lu, C. Shao, F. Ruan, D. Yu, M. Li, W. Zhan, D. K. Torpokov, and D. Nikolenko, Test results of the HIRFL-CSR cluster target, Nucl. Instrum. Methods Phys. Res., Sect. A **555**, 15 (2005).

[8] Th. Stöhlker *et al.*, Charge-exchange cross sections and beam lifetimes for stored and decelerated bare uranium ions, Phys. Rev. A **58**, 2043 (1998).

[9] F. M. Kröger *et al.*, Electron capture of Xe^{54+} in collisions with H_2 molecules in the energy range between 5.5 and 30.9 MeV/u, Phys. Rev. A **102**, 042825 (2020).

[10] B. Yang *et al.*, Alignment of the projectile $2p_{3/2}$ state created by nonradiative electron capture in 95- and 146-MeV/u Xe^{54+} with Kr and Xe collisions, Phys. Rev. A **102**, 042803 (2020).

[11] B. Yang *et al.*, State-selective nonradiative electron capture in collisions of 95–197-MeV/u Xe^{54+} with Kr and Xe, Phys. Rev. A **104**, 032815 (2021).

[12] B. Yang *et al.*, Nearly isotropic Lyman-α_1 radiation $2p_{3/2} \rightarrow 1s_{1/2}$ following nonradiative electron capture in $Xe^{54+} + Kr$ collisions at 197 MeV u^{-1}, J. Phys. B: At., Mol. Opt. Phys. **56**, 055203 (2023).

[13] X. Ma, Th. Stöhlker, F. Bosch, O. Brinzanescu, S. Fritzsche, C. Kozhuharov, T. Ludziejewski, P. H. Mokler, Z. Stachura, and A. Warczak, State-selective electron capture into He-like U^{90+} ions in collisions with gaseous targets, Phys. Rev. A **64**, 012704 (2001).

[14] Th. Stöhlker, C. Kozhuharov, P. H. Mokler, R. E. Olson, Z. Stachura, and Z. Warczak, Single and double electron-capture in collisions of highly ionized, decelerated Ge ions with Ne, J. Phys. B: At., Mol. Opt. Phys. **25**, 4527 (1992).

[15] H. Imao *et al.*, Charge stripping of ^{238}U ion beam by helium gas stripper, Phys. Rev. Spec. Top.–Accel. Beams **15**, 123501 (2012).

[16] J. Eichler, Relativistic eikonal theory of electron capture, Phys. Rev. A **32**, 112 (1985).

[17] R. Anholt and J. Eichler, Eikonal calculations of electron-capture by relativistic projectiles, Phys. Rev. A **31**, 3505 (1985).

[18] N. Toshima and J. Eichler, Coupled-channel theory of excitation and charge-transfer in relativistic atomic collisions, Phys. Rev. A **38**, 2305 (1988).

[19] N. Toshima, T. Ishihara, and J. Eichler, Distorted-wave theories for electron-capture and the associated high-energy behavior of cross sections, Phys. Rev. A **36**, 2659 (1987).

[20] R. E. Olson, *Springer Handbook of Atomic, Molecular and Optical Physics* (Springer, New York, 2006).

[21] J. H. McGuire and L. Weaver, Independent electron approximation for atomic scattering by heavy particles, Phys. Rev. A **16**, 41 (1977).

[22] W. E. Meyerhof, R. Anholt, X. Y. Xu, H. Gould, B Feinberg, R. J. McDonald, H. E. Wegner, and P. Thieberger, Multiple ionization and capture in relativistic heavy-ion atom collisions, Nucl. Instrum. Methods Phys. Res., Sect. A **262**, 10 (1987).

[23] R. Anholt *et al.*, Atomic collisions with relativistic heavy ions: Target inner-shell ionization, Phys. Rev. A **30**, 2234 (1984).

[24] C. Shao *et al.*, Production and decay of *K*-shell hollow krypton in collisions with 52–197-MeV/u bare xenon ions, Phys. Rev. A **96**, 012708 (2017).

[25] G. Bednarz *et al.*, Double-electron capture in relativistic U^{92+} collisions at the ESR gas-jet target, Nucl. Instrum. Methods Phys. Res., Sect. B **205**, 573 (2003).

[26] A. Simon, A. Warczak, T. ElKafrawy, and J. A. Tanis, Radiative double electron capture in collisions of O^{8+} ions with carbon, Phys. Rev. Lett. **104**, 123001 (2010).

[27] A. Warczak *et al.*, Radiative double-electron capture in heavy-ion atom collisions, Nucl. Instrum. Methods Phys. Res., Sect. B **98**, 303 (1995).

[28] D. R. Plante, W. R. Johnson, and J. Sapirstein, Relativistic all-order many-body calculations of the $n = 1$ and $n = 2$ states of heliumlike ions, Phys. Rev. A **49**, 3519 (1994).

[29] W. R. Johnson and G. Soff, The Lamb shift in hydrogen-like atoms, $1 \leqslant Z \leqslant 110$, At. Data Nucl. Data Tables **33**, 405 (1985).

[30] M. O. Herdrich *et al.*, High-resolution x-ray emission study for Xe^{54+} on Xe collisions, Eur. Phys. J. D **77**, 125 (2023).

[31] Th. Stöhlker *et al.*, Strong alignment observed for the time-reversed photoionization process studied in relativistic collisions with bare uranium ions, Phys. Rev. Lett. **79**, 3270 (1997).